Hindawi
Geofluids
Volume 2022, Article ID 2954973, 9 pages
https://doi.org/10.1155/2022/2954973

Research Article

Theoretical Research on the Movement Law of Water Cone Behavior in Heavy Oil Reservoirs with Bottom Water

Kai Wang[1], **Chenyang Tang**[1], **Tianyou Zhang**[1], **Yufei Gao**[1], **Jingyun Zou**[1], **Yan Jiang**[2], **Kuo Sun**[1] and **Yan Chen**[1]

[1]*China National Offshore Oil Corporation Research Institute, Beijing 100028, China*
[2]*Engineering Technology Research Institute of PetroChina Huabei Oilfield Company, Hebei 062552, China*

Correspondence should be addressed to Kai Wang; wangkaiupc@163.com

Received 23 January 2022; Accepted 27 April 2022; Published 17 June 2022

Academic Editor: Jinjie Wang

Aiming at the unclear reorganization of a water cone shape, its sweep range, and water saturation distribution of horizontal well in heavy oil reservoirs with bottom water, a mathematical method was proposed in this paper to establish a microtube model and physical model with the starting pressure gradient (SPG) to study the water cone behavior. The results showed that the different water-cut stage, mobility, depth from oil-water interface (DOWI), and liquid production strength have an obvious impact on water cone behavior. Moreover, we found an interesting phenomenon on an extreme point in water saturation derivation among water cone, which could be a reason for further adjustment. Finally, we confirmed the calculation results with physical simulation, which is highly consistent. The new method proposed in this paper was significant in the water cone behavior study and has a broad application in heavy oil reservoir development in the future.

1. Introduction

The development of heavy oil reservoirs with bottom water is one of the big challenges in the oil and gas exploitation field worldwide [1, 2]. Developing reservoirs of this type often shows early water appearance, short water-free period, high water-cut ratio, and even violent water-cut ratio after water breakthrough, which reduces oil recovery and increases oilfield production risk [3, 4].

The core technology for developing this type of reservoirs using horizontal wells exists in the description of the water cone. The evolution of the water cone and its sweeping range has a deep influence on the developing and of adjusting project design. In the past decades, many researchers have conducted experimental, analytical, and numerical studies in the water cone behavior of horizontal wells [5–7]. However, the results of different research methods varied largely, especially for heavy oil reservoirs. For example, the sweeping range from the laboratory experiment is much lower than that from numerical simulations, because the heavy oil reservoir is similar to the low permeability reservoir in the porous medium seepage, which is a non-Darcy flow with a starting pressure gradient (SPG) [8]. So, in heavy oil reservoirs, seepage can occur only if the production pressure gradient is greater than the SPG [9–11]. However, the existing commercial numerical simulation software, such as Eclipse CMG and Petrel Re, is all based on the Darcy seepage model and cannot directly characterize the non-Darcy flow in heavy oil reservoirs [12–16]. Moreover, there exists few theoretical research on the description of water cone behavior, not to mention the theoretical study considering the starting pressure gradient. All the problems mentioned above seriously influence the exact description of water cone behavior and its sweeping range in heavy oil reservoirs with bottom water, which have an impact on further development and adjustment of this type of reservoirs [17–19].

In this paper, we propose a new mathematical method to achieve the characterization of the water cone behavior in heavy oil reservoirs with bottom water. Then, we construct a microtube model and a physical model to observe the evolution of the water cone and sweeping range in this type of reservoir. The displacement path was divided through the

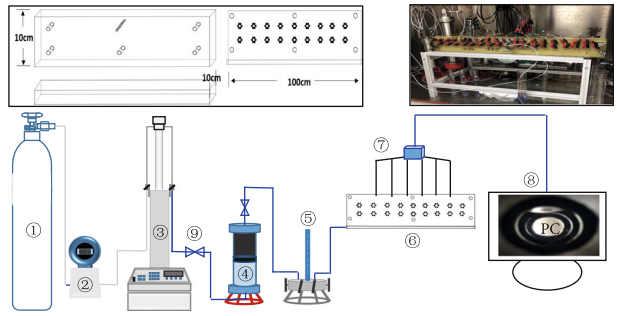

Figure 1: Models and experiment design of physical simulation.

analysis of the development process of the bottom water reservoir. Combined with the water-drive front equation, splitting flow equation, and Darcy equation, the expansion of the bottom water displacement area was obtained. Finally, the water cone radius, sweep range, and water saturation distribution in different positions were completely calculated. The new method proposed in this paper was significant in the water cone behavior study and has a broad application in heavy oil reservoir development in the future [20–23].

2. Models and Methods

2.1. Physical Model. The experimental setup of flowing tests consisted of a displacement pump (Teledyne ISCO, USA) used to inject fluids with different flow rates, two cylinders for formation water and model oil, an ultralarge 3D sand-pack model with a size of 100 cm×10 cm×10 cm, and a data collection system used to monitor saturation [24, 25]. Figure 1 shows a photograph of the designed 3D project, real 3D sand-pack model, and schematic of the experimental equipment, respectively. Figure 2 shows a seepage model. The similarity criteria and the main parameters are shown in Tables 1 and 2, respectively.

3. Results and Discussion

3.1. Influence of Water-Cut Stage Difference on the Water Cone Behavior. According to the above calculation process, when the mobility is 11, 33, and 64 mPa s, the movement of a water cone shape and sweeping range before and after water-drive front breakthrough were calculated, respectively, as shown in Figure 3. Meanwhile, the physical model was also simulated at the mobility of 64 mPa s, in order to calibrate the results.

The result shows that, with increasing mobility, the sweeping range of the water cone increases. From Figures 3(a) and 3(b), as the mobility increases from 11 to 64 mPa s, the water cone sweeping range increases from 60 m to 225 m. In the early stage, the movement of the water cone mainly focuses on the horizontal direction. But, after the water-drive front breakthrough, the movement of the water cone changed to a vertical direction. The water cone movement near the well was obvious while that far away from the well is limited.

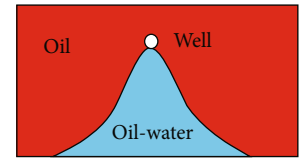

Figure 2: Seepage model.

From Figure 3(c), the ultralarge physical model presents the movement and water saturation distribution of the water cone at a mobility of 64 mPa s. The water cone movement shows a similar characterization with the calculated result, that is, moving horizontally firstly and then vertically. The sweeping efficiency was 0.35 initially and changed to 0.48 with water-cut reaching 98%. The distribution of water saturation through the monitor presents a relatively high value near the wellbore and a low value away from the wellbore. The reason lies in the distribution of the pressure difference on the plane. The closer it is to the well, the greater the pressure difference, and the higher the water saturation. The high water-cut was mainly contributed by the washing nearby the wellbore.

3.2. Influence of Mobility Difference on Water Cone Behavior. According to the above calculation process, the movement of the water cone behavior and the sweeping range were calculated, respectively, with the mobility ranging from 10 to $90 \times 10^{-3} \mu m^2/mPa\,s$. Meanwhile, the physical model with a similar principle was also conducted for the calibration of the water cone behavior and sweep range. The results are shown in Figures 4–6.

From Figures 4(a) and 4(b), with the mobility increasing or viscosity decreasing, the water cone radius increases. When the mobility changes from 10 to $90 \times 10^{-3} \mu m^2/mPa\,s$, the water cone radius increases from 48 m to 252 m. There exists a good relationship between water radius and mobility with a correlation coefficient of around 0.99.

From Figure 6, the physical simulation results showed that, with the increment of mobility, the water cone radius increased. When the mobility changes from 15 to $60 \times 10^{-3} \mu m^2/mPa\,s$, the water cone radius increases from 60 m to 200 m. The physical simulation results highly agreed with that of the calculation. In addition, all the physical simulation results showed a similar phenomenon as we discussed in

Table 1: Similarity criterion.

Classification	Criterion	Physical meaning
Geometric similarity	L_1/L_2	Ratio of length to width of the reservoir
	L_1/H	Ratio of reservoir length to thickness
	$\frac{L_1}{L_i}$	Ratio of reservoir length to horizontal well length
	$\Delta p/\rho_o gH$; $\Delta p/\rho_w gH$	The ratio of production pressure difference to gravity
Pressure similarity	$\Delta p/p_c$	The ratio of production pressure difference to capillary force
	$p_i/\bar{p}$	The ratio of reservoir pressure to the average pressure of the bottom layer
Physical similarity	ρ_o/ρ_w	Oil-water density ratio
	$K_{owe}\mu_w/K_{wor}\mu_o$	Oil to water mobility ratio
	S_{wc}/S_{or}, $1/S_{or}$	The prototype is similar to the model endpoint
	ϕ	Prototype is similar to model porosity
	C_t/C_o, C_o/C_w	The ratio of the comprehensive compression coefficient to the oil and water compression coefficient
Dynamic similarity	$KK_{wor}\Delta pt/\mu_w H^2\phi S_{wc}C_t P_i$, $\rho_w S_{wc}\phi L_l^2\mu_o/t\rho_o KK_{owc}\Delta p$	Darcy formula
	$L_1L_2KK_{wor}\rho_w g/\mu_w Q$, $L_1L_2KK_{wor}\Delta p/\mu_w QH$	Ratio of water influx to horizontal well production
	q_o/q_w	Ratio of oil to water production

Table 2: Parameter comparison of physical model with that of oilfield.

Parameter	Oilfield	Model
Thickness	20	10
Length	200	100
Width	20	10
Oil density	859.3	866.9
Water density	990	1000
Permeability	1200	2300
Pressure dropdown	3	0.006
Horizontal length	200	0.2
Well diameter	0.137	0.01
Oil production	1000	0.032

Section 3.1, that is, the distribution of water saturation through the monitor presents a relatively high value near the wellbore and a low value away from the wellbore.

From Figure 4(c), the distribution of water saturation at different positions in the water cone was calculated with oil viscosity ranging from 50 to 180 mPa s. The results showed that the water saturation in the water cone was high near the well and gradually decreased to the wings, indicating the law of first slowly declines, then rapidly declines, and finally slowly declines. With the decrease of oil viscosity, the water saturation at the same position increased, the viscosity is 50~180 mPa s, and the S_w at 100 m increased from 0.39 to 0.55. The reason lies in that the water saturation in the water cone at different positions was mainly affected by the flooding multiples. As shown in Figure 5, the relationship between water saturation and flooding multiples at different positions was calculated, which shows that there was a good linear relationship between them.

As shown in Figure 4(d), when the water saturation is derived from the water cone radius, the derivative curve presents an inverted bell shape, and an extreme point exists. The extreme point decreases with the increment of oil viscosity. When the oil viscosity was 50 mPa s, the extreme point was located at the water cone radius of 113 m. When the oil viscosity was 180 mPa s, the extreme point was located at the water cone radius of 55 m.

3.3. Influence of Distance from Oil-Water Interface (DOWI) on the Water Cone Behavior. According to the above calculation process, the water cone shape, water saturation distribution, and sweeping radius were calculated when the DOWI was 10, 15, and 20 m, respectively. The results are shown in Figure 7.

From Figure 7(a), when the DOWI is between 10 and 20 m with a fixed mobility at $33 \times 10^{-3}\mu m^2$/mPa s, the water cone radius ranged from 142 to 150 m. For heavy oil reservoirs with thin bottom water, the influence of DOWI is limited. As shown in Figure 7(b), the higher the mobility, the higher the influence of DOWI. When the mobility increases to 90 with DOWI between 10 and 20 m, the water cone radius ranged from 231 to 252 m. When the mobility was 11 with the DOWI between 10 and 20 m, the water cone radius ranged only from 56 to 58 m. In Figure 7(c), the law of water saturation distribution was similar to that described in Section 3.2. However, with the increase of DOWI, the water cone radius slightly decreased, and the water saturation at the same position increased due to the increase of

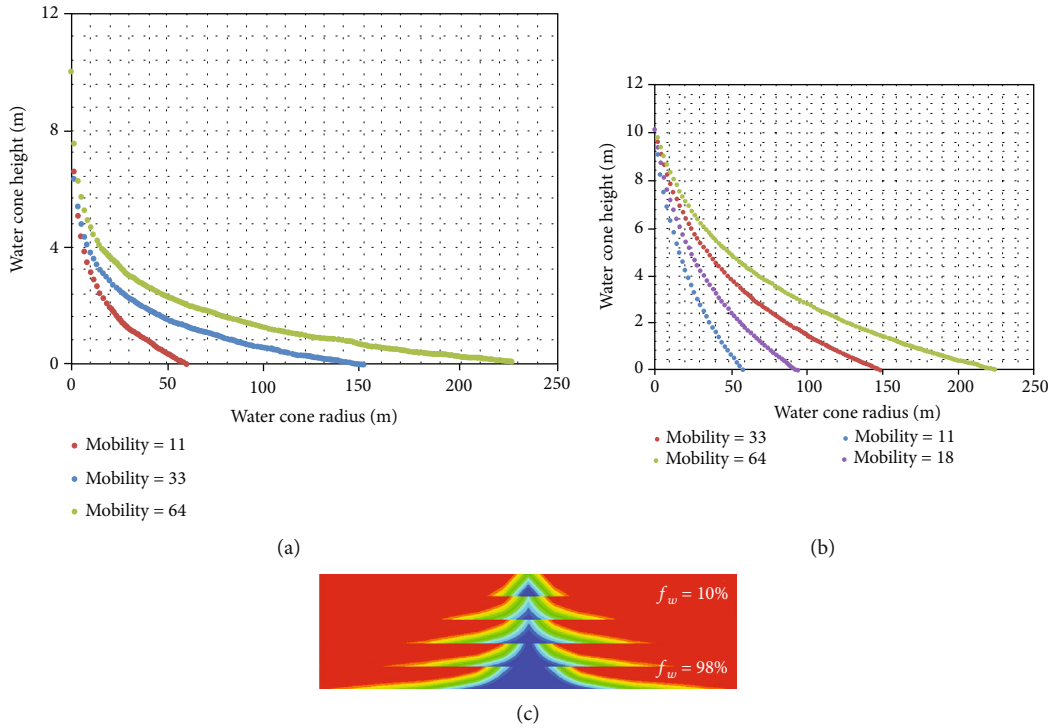

FIGURE 3: The influence of different water-cut stages on water cone behavior through mathematical calculation and physical simulation.

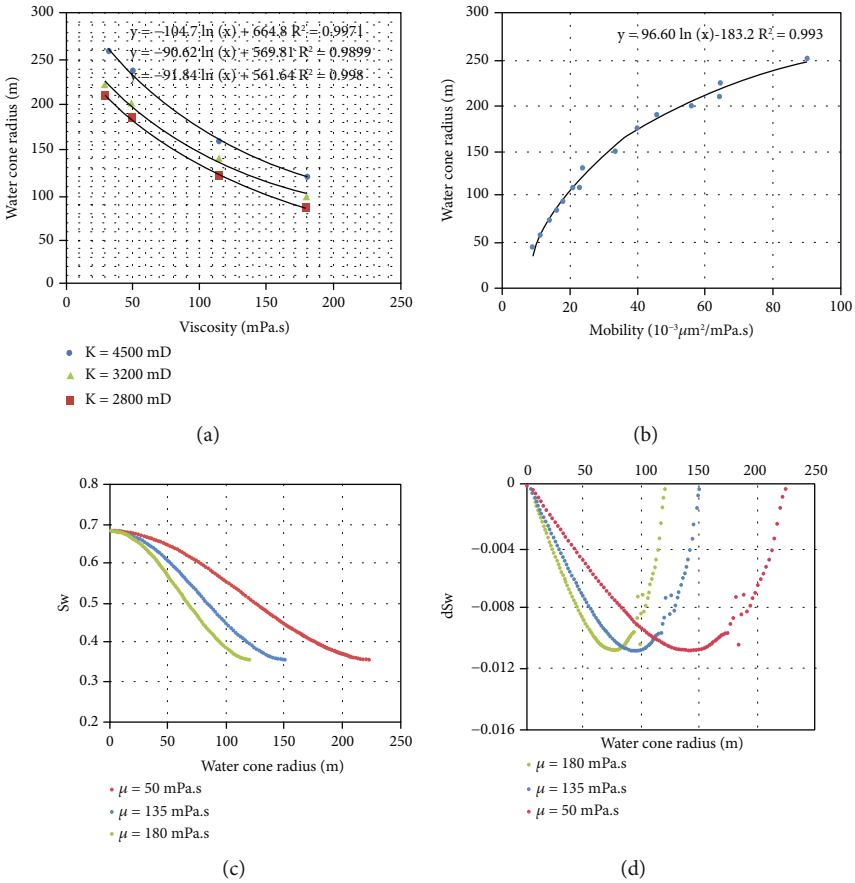

FIGURE 4: Influence of mobility on water cone behavior.

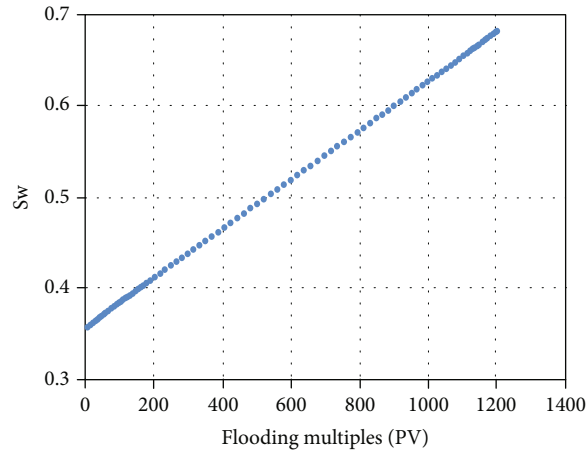

Figure 5: The relationship between S_w and flooding multiples.

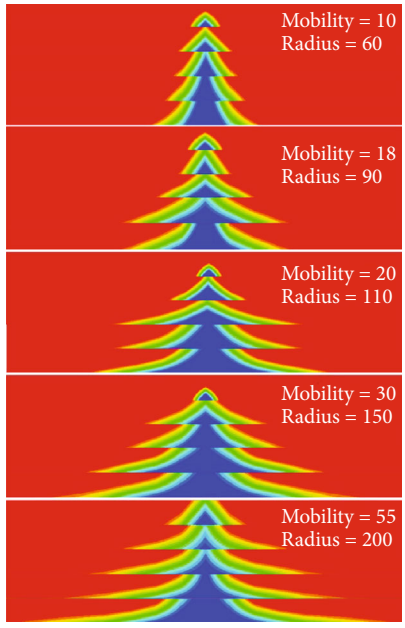

Figure 6: Physical simulation of water cone behavior under different mobility.

flooding multiples. As shown in Figure 7(d), the variation range of the water cone radius was limited with DOWI ranging from 10 to 20 m, and the extreme points were also highly concentrated, around 85 m.

3.4. Influence of Liquid Production Strength on Water Cone Behavior. According to the above calculation process, the water cone shape, water saturation distribution, and sweeping radius were calculated when the liquid production strength was 300, 500, and 1500 m^3/d, respectively. The results are shown in Figure 8.

As shown in Figure 8(a), when the liquid production strength was 300~1000 m^3/d with a fixed mobility of $33 \times 10^{-3} \mu m^2$/mPa s, the water cone radius was 100 to 150 m. For heavy oil reservoirs with thin bottom water, the liquid production strength had an obvious influence on the water cone shape and sweep radius. From Figure 8(b), when the liquid production strength was higher than 1000 m^3/d, the increase of water cone radius decreased under any mobility condition. In addition, with the increment of liquid production strength, the variation ranges of the water cone radius increased. When the liquid production strength increased from 300 to 1000 m^3/d with a fixed mobility of 11, the water cone radius increased from 30 to 58 m; when the mobility was 33, the water cone radius increased greatly from 100 m to 150 m; when the mobility was 65, the water cone radius increased from 160 m to 225 m. With the increased liquid production strength, the water saturation at the same position increased. From Figure 8(c), the strength increases from 300 to 1000 m^3/d, and the water saturation increases from 0.40 to 0.5 at 80 m, featured with decreasing slowly-rapidly-slowly. From Figure 8(d), the extreme point increased with the increment of the liquid production strength. When the liquid production strength is 300 m^3/d, the extreme point was located at 45 m. When the liquid production strength is 1000 m^3/d, it is located at 85 m.

3.5. Influence of Adjacent Well on the Water Cone Behavior. According to the calculation process in this paper, a model was built with DOWI of 10 m, permeability of 4500 md, oil viscosity of 135 mPa s, and liquid production strength of 1000 m^3/d. The movement of the water cone behavior and water saturation were calculated when two horizontal wells crossed at different positions. The influence degree was determined by Equation (1) to calculate the cumulative oil production. The results are shown in Figure 9.

$$\mathrm{MAX}\{S1 \times (Sw1 - Sw0) + S2 \times (Sw1 - Sw2) - S2 \times (Sw2 - Sw0)\}. \quad (1)$$

From Figure 10, two water cones with a radius of 150 m are crossed by different well spacings of around 120 m, 85 m, and 75 m, respectively. Then the movement of water cone behavior was calculated after crossing. It can be seen that with the reduction of well spacing, the uplift of water cone between wells was more and more obvious, and the

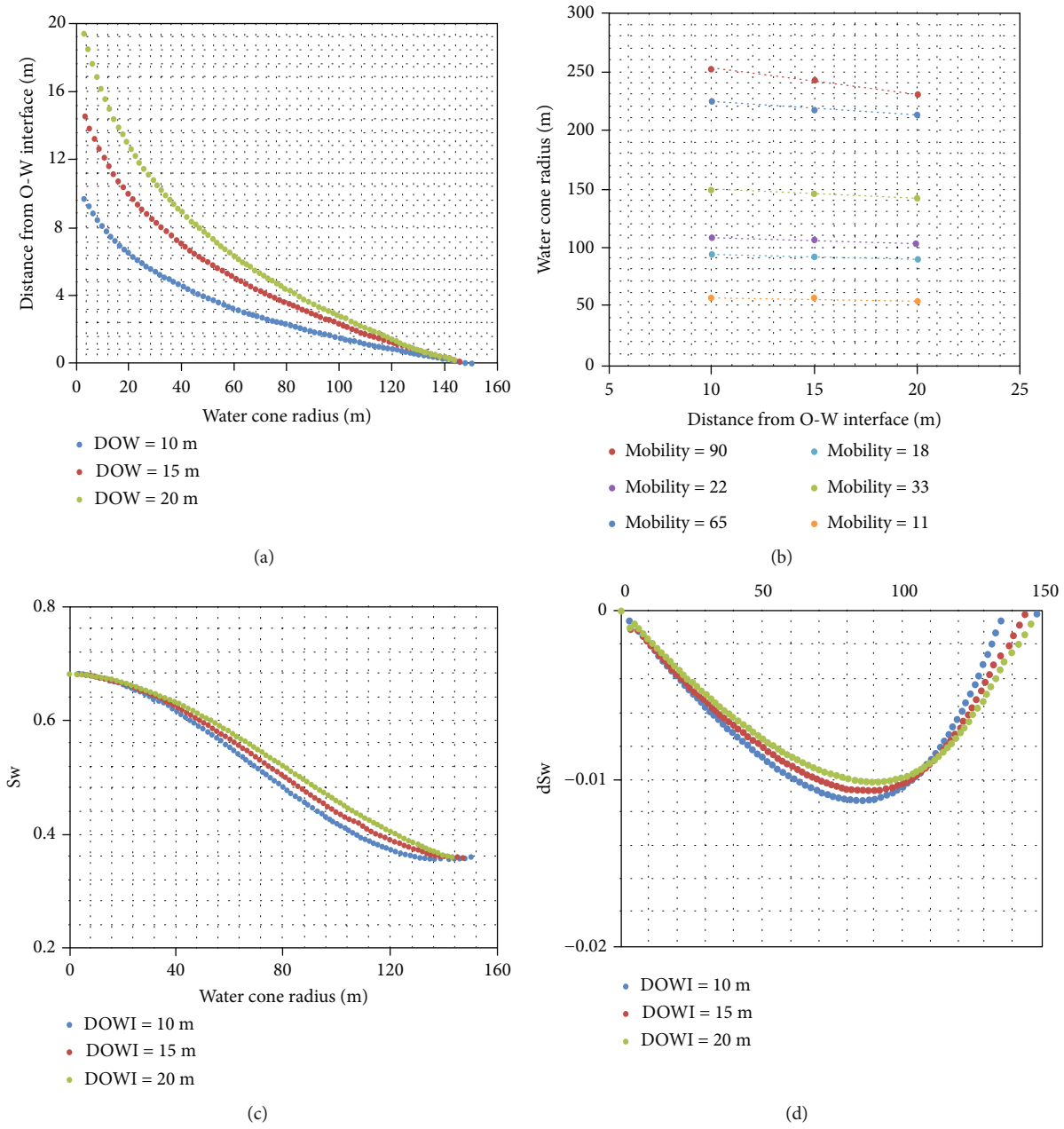

Figure 7: Influence of DOWI on water cone behavior.

remaining oil between wells was reduced, for the flooding multiples of the overlapping area were increased due to the joint action of two wells.

From Figure 10, the water saturation distribution between two water cones was calculated. As shown in Figure 10, with the reduction of well spacing, the water saturation in the overlapping area rises rapidly due to the joint flooding of two wells. The water saturation in the overlapping area was 0.4 when the water cone crossed at 120 m. When the overlapping area decreased to 85 m, the water saturation in the overlapping area rises to 0.6. When the well spacing further shortens, the water saturation rises to 0.68 due to the overlapping area being further flooded.

From Figure 11, the addition of an adjacent well had an obvious effect on the shape and water saturation distribution between water cones. Consistent with the calculated results, the water cone between two wells rises, and the water saturation increases. The closer the two wells, the higher the water cone, and water saturation rises due to the high-multiple flooding. The physical results confirmed what was obtained in the calculation process.

As shown in Figure 12(a), with the increment of well spacing, the cross-section oil increment first increased and then decreased. There exists a maximum cross-section oil increment. Moreover, there exists an interesting phenomenon, by comparing the intersection point of the maximum

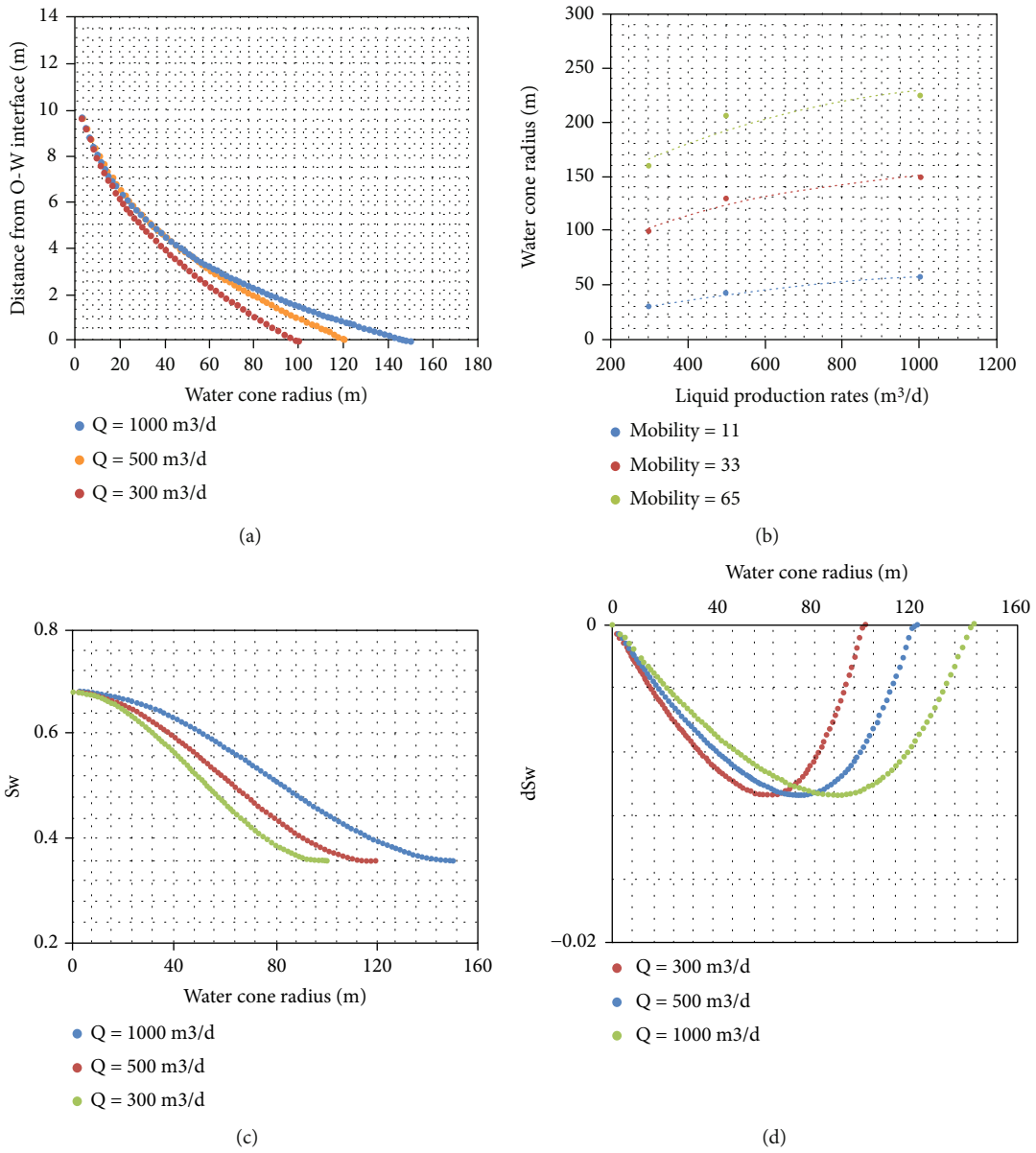

Figure 8: Influence of liquid production strength on the water cone behavior.

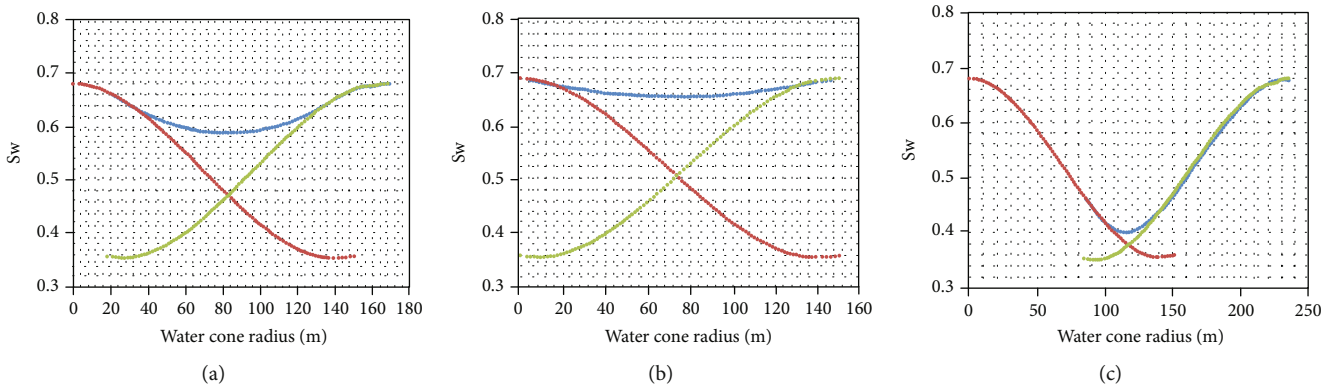

Figure 9: Influence of an adjacent well on the water cone behavior.

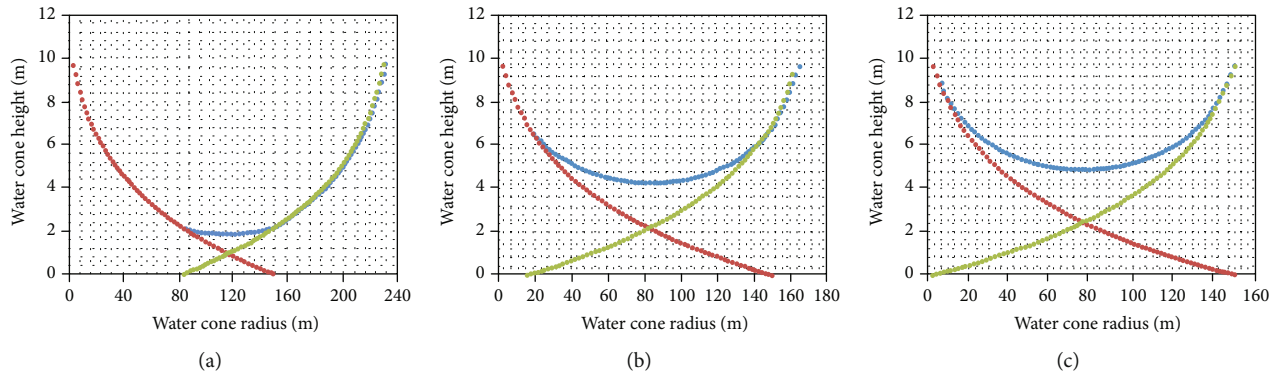

Figure 10: Influence of an adjacent well on the water saturation distribution in the water cone.

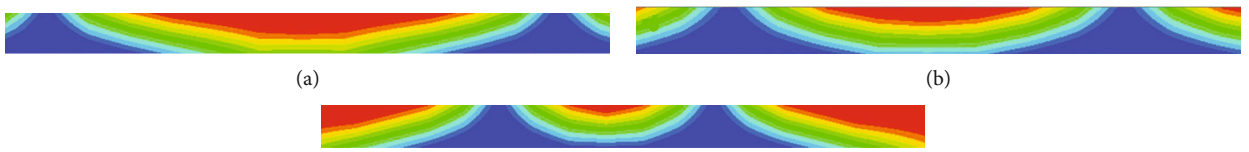

Figure 11: Influence of an adjacent well on the shape and water saturation distribution in the water cone through physical simulation.

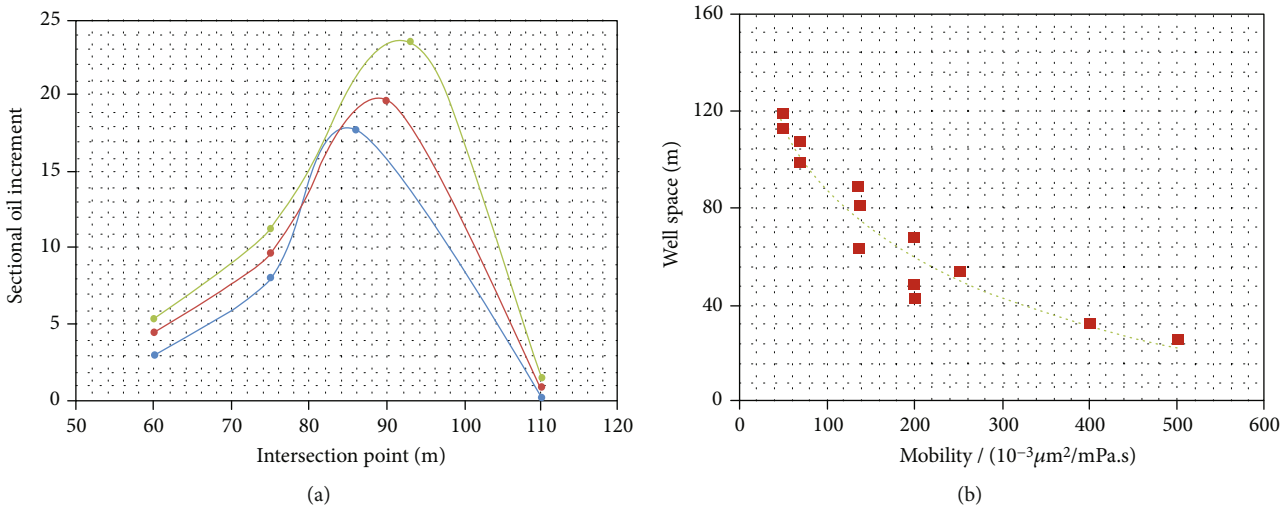

Figure 12: Relationship between well space and mobility.

cross-section oil increment with the extreme value of water saturation derivation in the water cone; it can be found that the two points are consistent. It provides a theoretical basis for optimizing reasonable well spacing in heavy oil reservoirs with bottom water. Figure 12(b) shows the relationship between optional well space and mobility. With the increase of oil viscosity, the reasonable well spacing decreases. When the viscosity was 100 mPa s, the optimized reasonable well spacing is 176 m. When the viscosity increases to 200 mPa s, the reasonable well spacing decreases to 120 m. With the increase of crude oil viscosity, the sweep range of the water cone decreases, which leads to a decrement in reasonable well spacing.

4. Conclusions

In this work, combined with the water-drive front equation, splitting flow equation, and Darcy equation, the movement of water cone behavior, its sweep range, and water saturation distribution were investigated. The summary was as follows:

(1) The water cone shape, its sweep range, and water saturation distribution were first studied through the seepage theory considering the starting pressure gradient. The influence of the different water-cut stage, DOWI, and liquid production strength was discussed in detail and showed a good relationship

(2) An interesting phenomenon was first found in this paper; there exists an extreme point in water saturation derivation in the water cone. It has a significant and theoretical meaning for the further adjustment

(3) Ultralarge scale physical simulation was conducted firstly in this paper, to explore the movement behavior, sweep range, and water saturation distribution of water cone

Data Availability

The data used to support the findings of this study are included within the article.

Conflicts of Interest

The authors declare that they have no conflicts of interest.

Acknowledgments

The second author and the first author contributed equally to this paper. The second institution and the first institution contributed equally to this paper.

References

[1] Q. You, Q. Wen, J. Fang, M. Guo, Q. Zhang, and C. Dai, "Experimental study on lateral flooding for enhanced oil recovery in bottom- water reservoir with high water cut," *Journal of Petroleum Science and Engineering*, vol. 174, pp. 747–756, 2019.

[2] G. Zhao, C. Dai, C. Gu, Q. You, and Y. Sun, "Expandable graphite particles as a novel in-depth steam channeling control agent in heavy oil reservoirs," *Chemical Engineering Journal*, vol. 368, pp. 668–677, 2019.

[3] D. U. Yu hong, "Study on enhanced oil recovery of Ren 11 fractured bottom water reservoir by gas injection," *Acta Petrolei Sinica*, vol. 26, no. 2, pp. 80–84, 2005.

[4] A. E. Gill, "Circulation and bottom water production in the Weddell Sea," *Deep-Sea Research and Oceanographic Abstracts*, vol. 20, no. 2, pp. 111–140, 1973.

[5] M. Tagavifar, R. Fortenberry, E. de Rouffignac, K. Sepehrnoori, and G. A. Pope, "Heavy-oil recovery by combined hot water and alkali/cosolvent/polymer flooding," *SPE Journal*, vol. 21, no. 1, pp. 74–86, 2016.

[6] J. Moortgat and A. Firoozabadi, "Water coning, water, and CO_2 injection in heavy-oil fractured reservoirs," *SPE Reservoir Evaluation & Engineering*, vol. 20, no. 1, pp. 168–183, 2017.

[7] A. Zakerian, S. Sarafraz, A. Tabzar, N. Hemmati, and S. R. Shadizadeh, "Numerical modeling and simulation of drilling cutting transport in horizontal wells," *Journal of Petroleum Exploration & Production Technology*, vol. 8, no. 2, pp. 455–474, 2018.

[8] O. Weiping, S. Hedong, and Z. Mian, "Well test analysis for multistage fractured horizontal wells in tight gas reservoir considering stress sensitivity," *Acta Petrolei Sinica*, vol. 39, no. 5, pp. 570–577, 2018.

[9] K. Wang, K. Li, Y. Gao, Y. Pan, and Q. You, "Research on water cone behavior in a heavy oil reservoir with bottom water considering the starting pressure gradient," *ACS Omega*, vol. 5, no. 27, pp. 16841–16847, 2020.

[10] H. Wang, X. Liao, N. Lu, Z. Cai, C. Liao, and X. Dou, "A study on development effect of horizontal well with SRV in unconventional tight oil reservoir," *Journal of the Energy Institute*, vol. 87, no. 2, pp. 114–120, 2014.

[11] W. Kai, Z. Yan, Z. Wensheng et al., "Study on the time-variant rule of reservoir parameters in sandstone reservoirs development," *Energy Sources Part A Recovery Utilization and Environmental Effects*, vol. 23, pp. 1–18, 2020.

[12] T. Engler and D. Tiab, "Analysis of pressure and pressure derivative without type-curve matching, 6. Horizontal well tests in anisotropic media," *Journal of Petroleum Science & Engineering*, vol. 15, no. 2–4, pp. 153–168, 1996.

[13] Y. L. Zhao, L. H. Zhang, J. X. Luo, and B. N. Zhang, "Performance of fractured horizontal well with stimulated reservoir volume in unconventional gas reservoir," *Journal of Hydrology*, vol. 512, no. 10, pp. 447–456, 2014.

[14] Y. C. Zeng, Z. Su, and N. Y. Wu, "Numerical simulation of heat production potential from hot dry rock by water circulating through two horizontal wells at desert peak geothermal field," *Energy*, vol. 56, no. 63, pp. 92–107, 2013.

[15] C. Dai, K. Wang, Y. Liu, H. Li, Z. Wei, and M. Zhao, "Reutilization of fracturing flowback fluids in surfactant flooding for enhanced oil recovery," *Energy & Fuels*, vol. 29, no. 4, pp. 2304–2311, 2015.

[16] Q. Sang, Y. Li, L. Yu, Z. Li, and M. Dong, "Enhanced oil recovery by branched-preformed particle gel injection in parallel-sandpack models," *Fuel*, vol. 136, pp. 295–306, 2014.

[17] C. Chen, J. Wan, and H. Zhan, "Theoretical and experimental studies of coupled seepage-pipe flow to a horizontal well," *Journal of Hydrology*, vol. 281, no. 1-2, pp. 159–171, 2003.

[18] R. Zhu and L. Tao, "Boundary element method of free boundary issues of stationary water cone for gas well," *Natural Gas Industry*, vol. 24, no. 12, pp. 93–95, 2004.

[19] N. Esmail, "Flow enhancement of medium-viscosity crude oil," *Petroleum Science & Technology*, vol. 24, no. 8, pp. 985–999, 2006.

[20] H. L. J. Gong, "The pressure effect on rheological behavior of water content of waxy crude oil," *Petroleum Science & Technology*, vol. 29, no. 13, pp. 1344–1352, 2011.

[21] W. C. Lee, Y. S. Lee, K. H. Kim, K. J. Lee, W. M. Sung, and J. Kim, "Investigation of gas and water coning behavior for the enhancement of oil production," *Korean Journal of Chemical Engineering*, vol. 28, no. 11, pp. 2102–2109, 2011.

[22] S. R. Heidemann, P. Lamoureux, and R. E. Buxbaum, "Growth cone behavior and production of traction force," *Journal of Cell Biology*, vol. 111, no. 5, pp. 1949–1957, 1990.

[23] G. S. Withers, C. D. James, C. E. Kingman, H. G. Craighead, and G. A. Banker, "Effects of substrate geometry on growth cone behavior and axon branching," *Developmental Neurobiology*, vol. 66, no. 11, pp. 1183–1194, 2006.

[24] Z. Peng, X. H. Wen, L. Ge, L. Bo, and M. S. Wei, "Existence of flow barriers improves horizontal well production in bottom water reservoirs," *SPE Conference*, vol. SPE115348, pp. 1–15, 2008.

[25] X. Tu, D. L. Peng, and Z. Chen, "Research and field application of water coning control with production balanced method in bottom-water reservoir," *SPE Conference*, vol. SPE105033, pp. 1–5, 2007.